Validating the performance of a Raman laser spectrometer (RLS) instrument under Martian conditions

Motamedi Mohammadabadi, K.

2013

document version
Publisher's PDF, also known as Version of record

Chapter 5: Raman study of hydrated sulphates and carbonates under Martian conditions with the RLS instrument

This chapter is the basis of a manuscript that will be submitted to the journal of Raman spectroscopy.
K. Motamedi, A. Colin, J.H. Hooijschuur, G.R. Davies.

Contents

5.1 Introduction

One of the main scientific objectives of the forthcoming ExoMars mission is the search for definitive signs of past or present life. A key goal of the mission will be to obtain more information about the current and past distribution of water on Mars. Evidence of the past liquid water activity has been found in multiple areas such as the Meridiani Planum region explored by the Opportunity rover. Observation of the layered sedimentary rocks show that these rocks contain high (30%– 40%) abundances of sulphates (mostly jarosite) (Christensen et al., 2004) likely formed by the evaporation of sulphur-rich water (Squyres et al., 2004). Sulphates were also observed from orbit instruments in the layered deposits of Valles Marineris as well as in more local locations such as crater interiors (Langevin et al., 2005).

Carbonates are expected weathering products of water and basalt in a CO_2 rich atmosphere (Gooding, 1978; Catling, 1999). The presence of carbonates as well as accompanying clays on Mars suggest that water was neutral to alkaline at the time during the Noachian era (Fairen et al., 2004). According to the recent data, carbonates exist locally on Martian surface and in veins within Martian meteorites (Bridges et al., 2001) and possibly at < 5% abundance in Mars dust (Bandfield et al., 2003).

Laboratory studies demonstrate that the Martian meteorites contain sulphur and water bearing minerals such as amphiboles. The discovery of hydrated minerals in meteorites was the first unambiguous evidence of a hydrous history of Mars. The discovery of sulphur determines that the abundant sulphur on the surface of Mars is due largely to chemical reactions in the Martian atmosphere that are similar to those that occur in Earth atmosphere. Therefore in order to understand the history of water on Mars current and future missions aim to identify carbonate and hydrated minerals and determine the geologic environments and processes responsible for their formation. Consequently, analysis of carbonate and hydrated minerals is a fundamental goal of the ExoMars mission to enable assessment of the geological and climatic history and possible past and present 'habitability' of Mars. Therefore it is vital that a full assessment is made as to the potential of the RLS instrument to detect carbonate and hydrated minerals under Martian conditions. This chapter examines the capability of the RLS instrument to detect and distinguish between different hydrated sulphates and carbonates.

Our analyses were carried out with the RLS instrument. Raman spectroscopy is potentially a powerful method for structural and compositional characterization of minerals. To simulate Martian conditions our experiments were carried out in the Mars atmosphere simulation chamber (MASC). Our approach was initially to assess if the RLS instrument can provide Raman spectra on a series of natural carbonates and hydrated sulphates before assessing the effect of Martian condition (low pressure, 8 CO_2 mbar, temperatures at +10 and -20 °C) on the Raman peaks. As in previous chapters, key questions are therefore if Raman spectra are potentially influenced by a CO_2 atmosphere and low temperatures, down to -20 °C.

5.2 Analytical procedure

RLS instrument uses a laser with a ~ 659 nm laser with 20 mW output energy. The spectral resolution is ~ 4 cm^{-1} and the spectral range between ~ 187 and 3293 cm^{-1}. The data acquisition are performed for a single integration of 40 s. The Raman spectra are obtained with the RLS instrument at +10 and -20 °C. In most cases the minerals are also analysed using a commercial Renishaw InVia Raman microscope under laboratory conditions to provide high quality Raman spectra for comparison. The spectra resolution of Renishaw is ~ 3 cm^{-1}. We recorded data between 125 and 4000 cm^{-1} range with acquisition time of 10 s. This commercial spectrometer uses near infrared laser excitation at 785 nm. To ensure high quality data, the charge coupled detector (CCD) is cooled to -70 °C.

5.2.1 Sample compositions

The compositions of the selected minerals are presented in Table 5.1.The EMPA data were collected on a JEOL JXA-8800M Superprobe at the VU University Amsterdam, the details information based on Electron microprobe analyser (EMPA) was presented in chapter four, section 4.3.1.

	Barite			Gypsum			Aragonite			Calcite		
	Weight%	STDEV	2σ	Weight%	STDEV	2σ	Weight%	STDEV	2σ	Weight%	STDEV	2σ
Na_2O	0.14	0.02	0.00	0.02	0.00	0.00	0.00	0.00	0.00	0.00	0.00	0.00
BaO	62.63	0.23	0.19	0.01	0.02	0.01	0.01	0.01	0.01	0.00	0.01	0.01
CaO	0.00	0.00	0.00	34.65	0.36	0.30	51.77	0.26	0.21	51.72	0.22	0.18
K_2O	0.00	0.01	0.00	0.01	0.01	0.01	0.00	0.00	0.00	0.00	0.00	0.00
SrO	0.01	0.02	0.02	0.02	0.02	0.01	0.33	0.16	0.13	0.00	0.00	0.00
SO_3	34.56	0.16	0.13	53.40	0.27	0.22	0.01	0.01	0.01	0.01	0.01	0.01
MnO	0.00	0.00	0.00	0.00	0.01	0.01	0.00	0.00	0.00	0.05	0.01	0.01
MgO	0.00	0.00	0.00	0.00	0.00	0.00	0.00	0.00	0.00	0.00	0.00	0.00
Total	97.35	0.26	0.21	88.11	0.30	0.24	52.13	0.23	0.19	51.79	0.23	0.18

Table 5. 1. Average compositions of barite, gypsum, calcite, aragonite by EMPA.

5.2.2 Raman analyses of hydrated sulphates: gypsum, barite and anglesite

On Earth sulphur (S) occurs as the pure element as well as in the sulphate (SO_4^{2-}) and sulphide (S^{2-}) form, producing minerals such as barite ($BaSO_4$) and pyrite (Fe_2S). Sulphur is one of the most reactive elements and can form covalent chemical bonds both with itself and with other elements. Sulphur easily enters solution where it forms sulphate complexes, which may ultimately precipitate as sulphates. On Earth, sulphates represent a large group of minerals that occur in different environments. For example, sulphates can appear as products of marine sediment formation. They are also common at Mid Ocean Ridges, which are the major cooling environments on Earth. Here anhydrite ($CaSO_4$) is precipitated from Ca rich

hydrothermal fluids when they mix with seawater (Haymon, 1983; Tivey and McDuff, 1990). Over time the physical conditions of a hydrothermal system evolve and anhydrite can be altered to gypsum ($CaSO_4 \cdot 2H_2O$), or dissolved as the temperature drops below 130 °C. Barite ($BaSO_4$) can also be found as a minor component of hydrothermal systems (Haymon and Kastner, 1981; Hannington and Scott, 1988).

The sulphate ion with a formula of SO_4^{2-} consists of a central sulphur atom surrounded by four equivalent oxygen atoms in a tetrahedral arrangement. The sulphur atom is in the 6+ oxidation state whereas the four oxygen atoms are each in the 2- state and therefore, sulphates create strong Raman signals (Griffith, 1970). The vibrations of the sulphate ion ($SO4^{2-}$) are ν_1 symmetric stretching, ν_2 symmetric bending, ν_3 asymmetric stretching and ν_4 asymmetric bending and these vibration modes are Raman active (Fig. 5.1). The stretching modes are usually monitored in the 950– 1200 cm^{-1} area, and the bending modes occur between 400 and 650 cm^{-1} area (Ramakrishnan et al., 1985). In a crystal structure the molecular vibration of SO_4^{2-} are under other influences from the cations, for instance Ba or Ca.

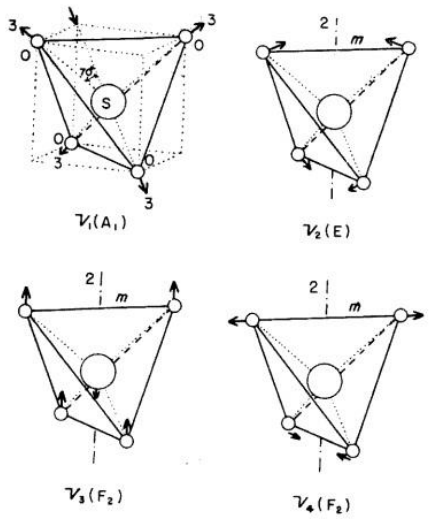

Figure 5. 1. The four vibration modes of sulphate ion SO_4^{2-} (Mitra and Gielisse, 1964).

For this study we have selected two of the most common sulphates that have relatively simple chemical compositions and mineral structures; barite and gypsum. In addition, sulphates that are geologically less common (e.g. anglesite) and phases that are more complex and more hydrated such as jarosite where also studied. We also examined polyhalite, epsomite, glauberite and coelestine. However, we could not obtain high quality RLS Raman spectra of these minerals as spectra show strong noise without any resolvable peaks. As explained in detail in chapter six, the current set up of the RLS instrument does not allow us to detect Raman peaks of OH vibration modes. Consequently, we focus on the Raman spectral region of

i) Fundamental vibrational modes of $(SO_4)^{2-}$
ii) Vibration modes of cation– O bonds from the interactions between the cation and O of either H_2O or SO_4^{2-} (Nakamoto, 2009)

5.2.3 Raman analyses of carbonates: calcite and aragonite

Based on the importance of detection of carbonate minerals on Mars (section 5.1), we have selected calcite and aragonite to analyse their RLS Raman spectra in MASC under Martian conditions. Calcite is one of the most common minerals on Earth, comprising about 4% by weight of the Earth's crust and it is formed in many different geological environments; sedimentary, igneous, and metamorphic rocks. The other selected sample, aragonite is formed by biological and physical processes, including precipitation from marine and freshwater environments (Brian et al., 1989). Aragonite is a polymorph of calcite, both having the chemical composition $CaCO_3$ but with a different molecular structure. Aragonite forms orthorhombic crystals, whereas calcite forms trigonal crystals. Raman spectroscopy is also capable of identifying polymorphs as the technique is based on distinguishing differences in molecular bonds. It should be kept in mind that Raman spectra mostly provide information on covalent bonds and that the Raman effect is very weak for ionic bonds. Importantly, the covalent bonding environment is influenced by cation substitution in a carbonate mineral structure and this enables different carbonates to be distinguished using the Raman spectroscopy.

The structure of the carbonate ion has two (long) single bonds that link carbon to negatively charged oxygen atoms, and one short double bond to a neutral oxygen (Fig. 5.2).

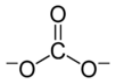

Figure 5.2. The structure of the carbonate ion

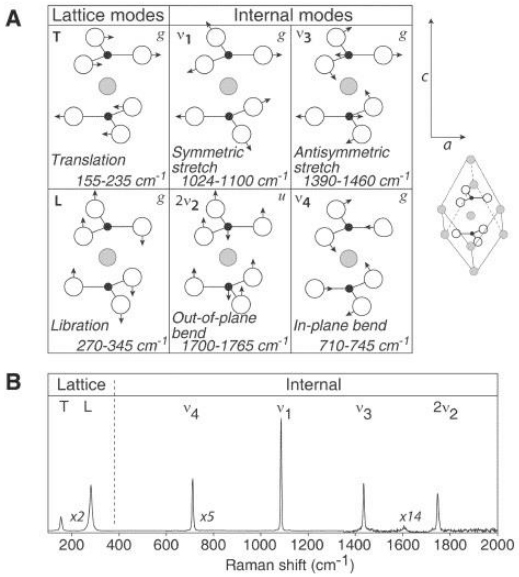

Figure 5.3. Raman peaks of the basic carbonate unit cell produced by lattice and internal modes (Buzgar and Apopei, 2009).

Raman spectra of the carbonate ion can be divided into two parts: lattice and internal modes (Fig. 5.3). Carbonate lattice vibration modes include translational and librational modes, which generate peaks with Raman shifts between 50 and 360 cm^{-1}. Internal vibration modes of the carbonate ion produce more intense Raman peaks. ν_1 is the most intense peak (at 1087 cm^{-1}) of the calcite spectrum and results from the symmetric stretching of CO_3 group. The ν_2 asymmetric bending vibration mode is not active in Raman. However, the peak $2\nu_2$ is an overtone of the first order ν_2 and detected between 1700 and 1765 cm^{-1}. ν_3 is related to the asymmetric stretching mode, 1437 cm^{-1} and ν_4 is attributed to a symmetric bending mode at 715 cm^{-1}. A weak peak detected at 1749 cm^{-1} is considered as a combination peak ($\nu_1 + \nu_4$) (Gunasekaran et al., 2006).

5.3 Renishaw data of hydrated sulphates and carbonates

In order to obtain Raman spectra under laboratory condition, selected minerals were placed on the polished stainless steel surface on the stage of the Renishaw microscope. We obtained Raman spectra with 20 X microscope objective. Raman spectra (obtain with the Renishaw InVia Reflex confocal Raman microscope) of gypsum, barite and anglesite (as representative sulphate samples) and calcite and aragonite (as representative carbonate samples) are presented in the following Figures. The data are presented in this section and discussed in details in the following sections.

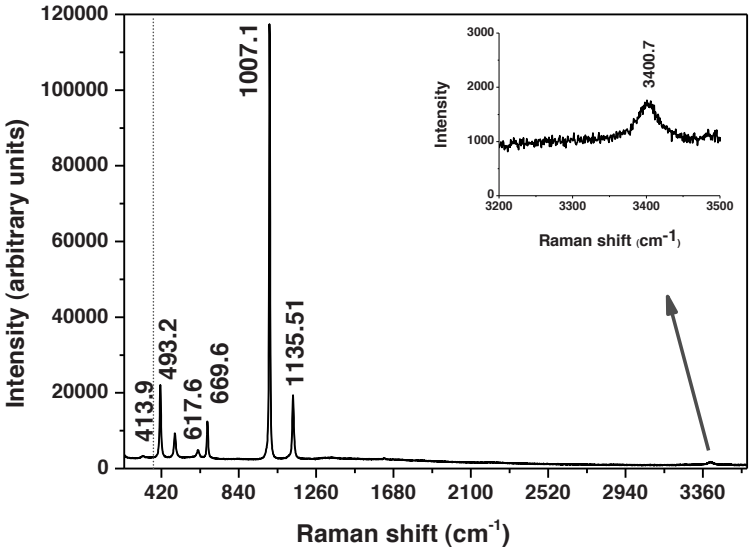

Figure 5.4. Gypsum Raman spectrum taken with the Renishaw InVia Reflex confocal Raman microscope. The peak at 3400.7 cm^{-1} is attributed to O─ H vibration mode of water in the gypsum structure. The Raman spectrum of gypsum is separated into two parts, external vibrations (< 400 cm^{-1}) and internal vibrations (400─ 1200 cm^{-1}) of the sulphate groups.

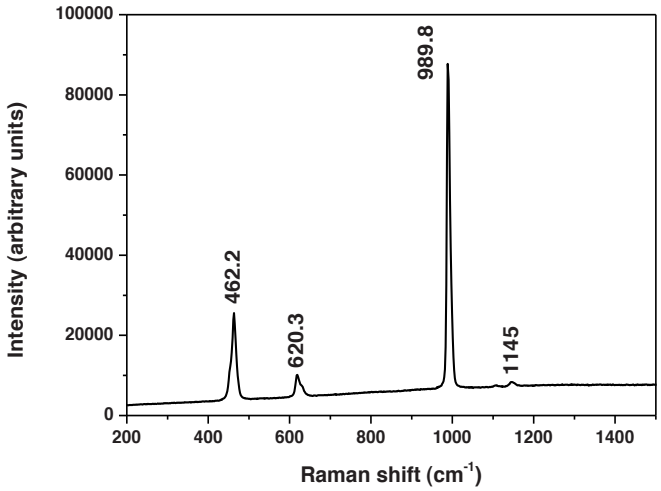

Figure 5.5. Barite Raman spectrum taken with the Renishaw InVia Reflex confocal Raman microscope.

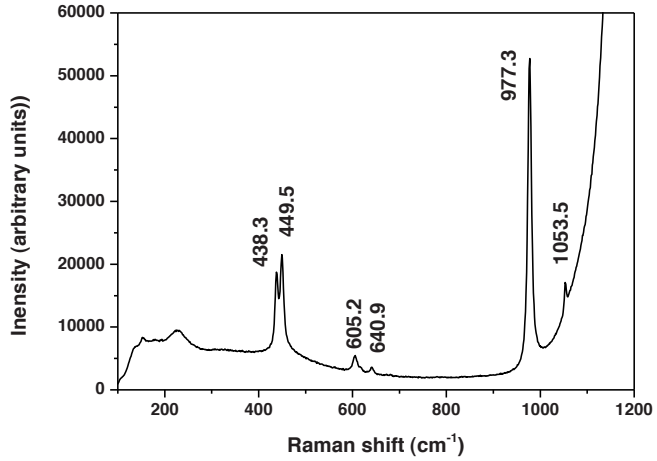

Figure 5.6. Anglesite Raman spectrum taken with the Renishaw InVia Reflex confocal Raman microscope.

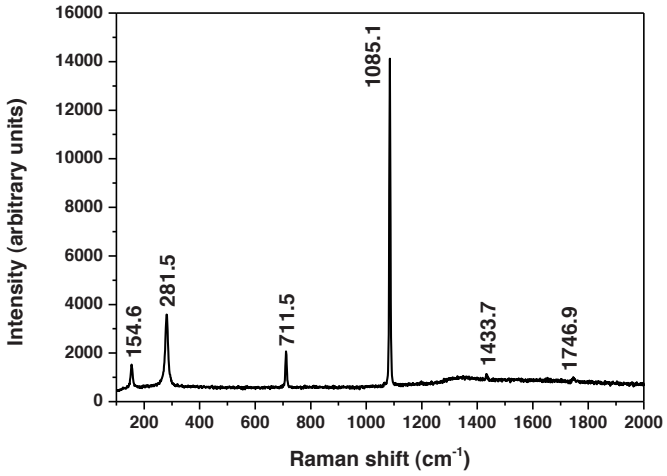

Figure 5.7. Calcite Raman spectrum taken with the Renishaw InVia Reflex confocal Raman microscope.

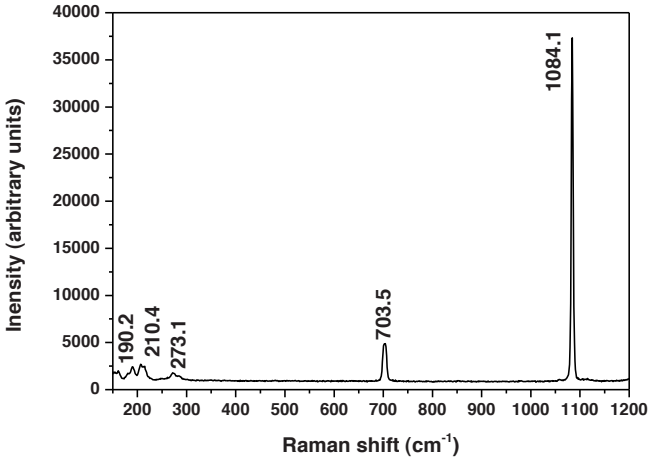

Figure 5.8. Aragonite Raman spectrum taken with the Renishaw InVia Reflex confocal Raman microscope.

5.4 RLS data of hydrated sulphates and carbonates samples

We acquired RLS Raman spectra of selected samples while MASC was under vacuum condition and sample temperatures were between 10 °C and -20 °C. In the next step, we obtained Raman spectra at -20 °C, while MASC was at 8 mbar CO_2. The RLS Raman spectra of gypsum, barite and anglesite (representing hydrated sulphate samples) and calcite and aragonite (representing carbonate samples) are presented in the following Figures:

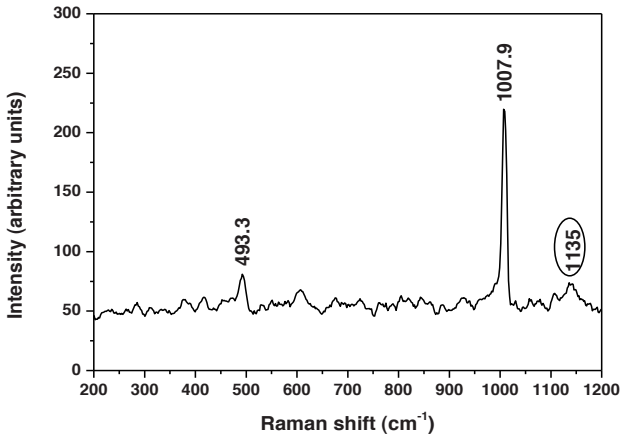

Figure 5.9. Gypsum RLS Raman spectrum under vacuum at 10 °C. The peak at ~ 1135 cm^{-1} is poorly resolved from the background noise.

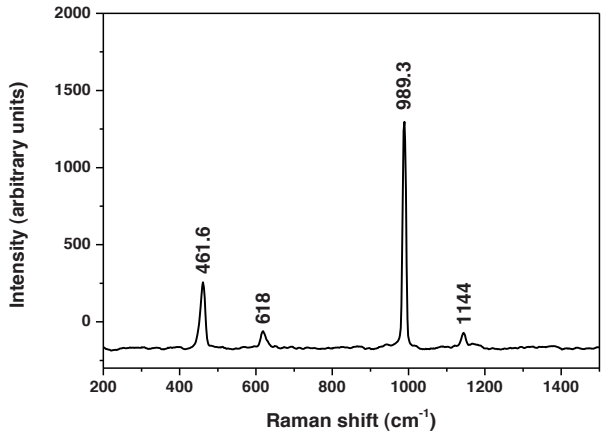

Figure 5.10. RLS Barite Raman spectrum under vacuum at 10 °C.

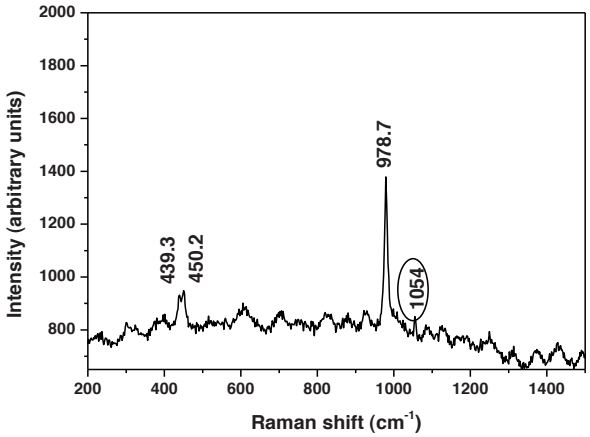

Figure 5.11. RLS anglesite Raman spectrum under vacuum at 10 °C. The possible peak at 1054 cm^{-1} was poorly resolved from the background at 10 °C.

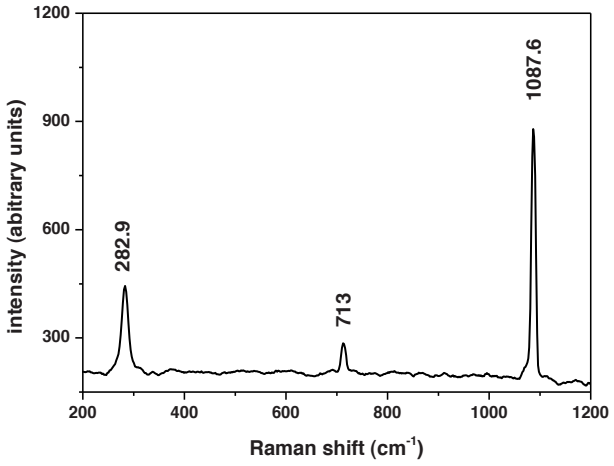

Figure 5.12. RLS calcite spectrum under vacuum at 10 °C.

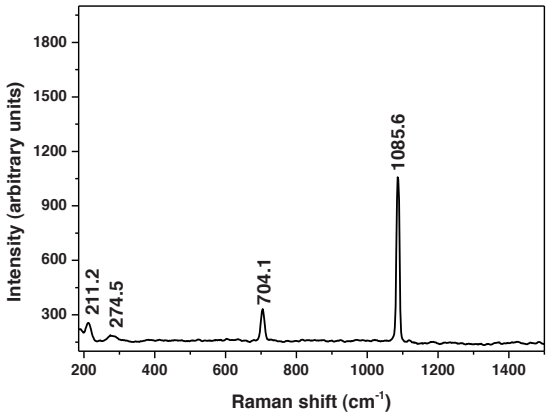

Figure 5.13. RLS aragonite Raman spectrum under vacuum at 10 °C.

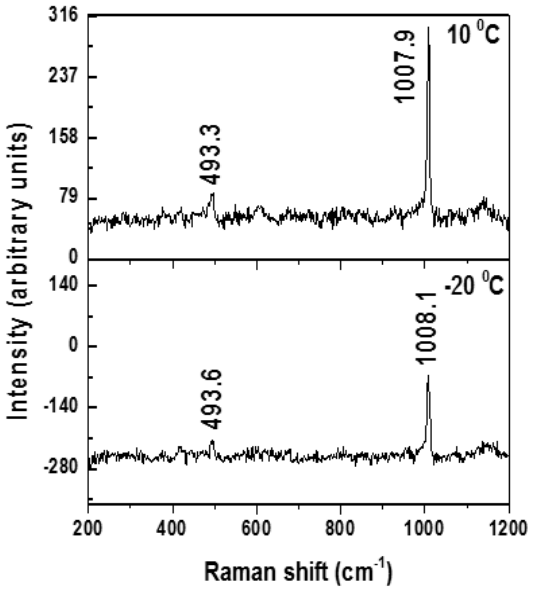

Figure 5.14. RLS Raman spectra of gypsum in the range 200– 12000 cm^{-1}, the measurement conditions are vacuum at +10 and -20 °C (the negative values are the result of temporal variation in the performance of the CCD. Backgrounds were determined for each specific analytical condition; e.g. +10 °C or -20 °C. In this specific case an unknown thermal perturbation of the CCD caused an over correction of the baseline during measurement at -20 °C).

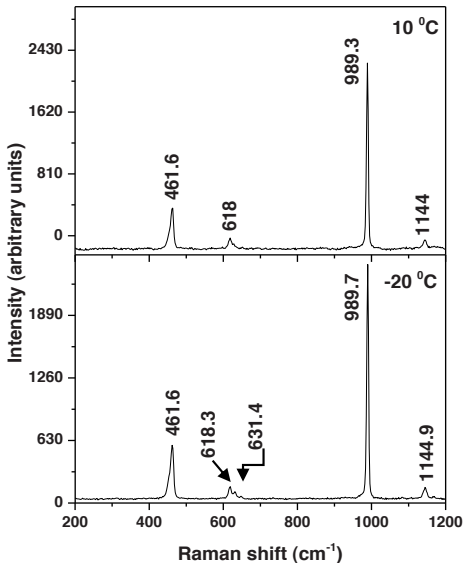

Figure 5.15. RLS Raman spectra of barite in the range 200– 12000 cm^{-1}, the measurement conditions are vacuum at +10 and -20 °C.

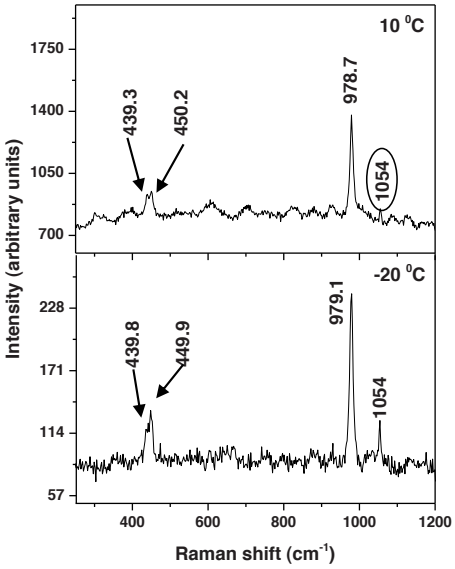

Figure 5.16. RLS Raman spectra of anglesite in the range 200– 12000 cm^{-1}, the measurement conditions are vacuum at +10 and -20 °C. The possible peak at 1054 cm^{-1} was poorly resolved from the background at 10 °C.

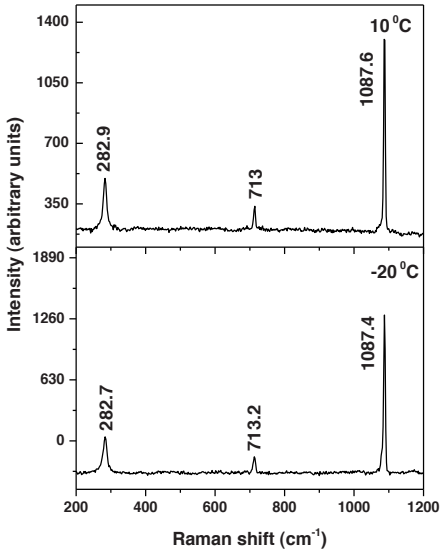

Figure 5.17. Raman spectra of calcite in the range 200– 12000 cm^{-1}, the measurement conditions are vacuum at +10 and -20 °C.

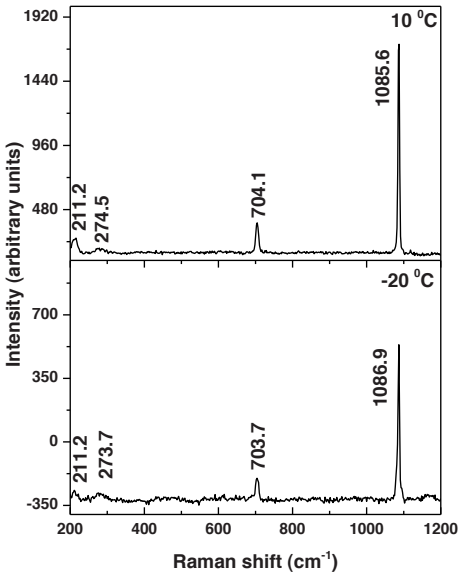

Figure 5.18. Raman spectra of aragonite in the range 200– 12000 cm^{-1}, the measurement conditions are vacuum at +10 and -20 °C.

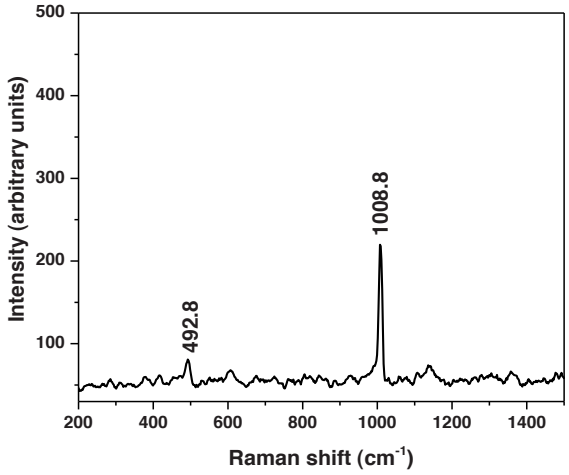

Figure 5.19. RLS gypsum Raman spectrum under 8 mbar CO_2 atmosphere at -20 °C.

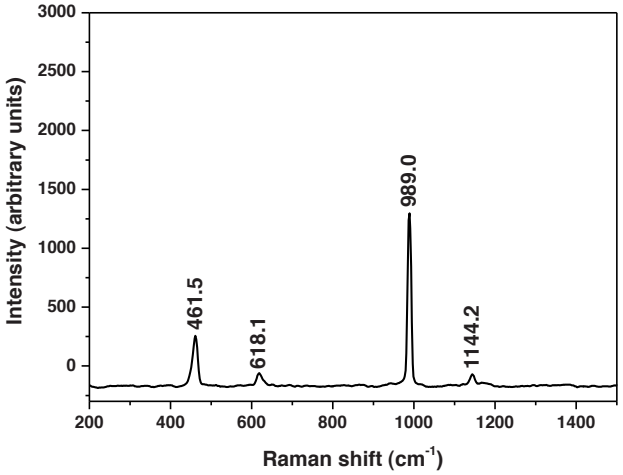

Figure 5.20. RLS barite Raman spectrum under 8 mbar CO_2 atmosphere at -20 °C.

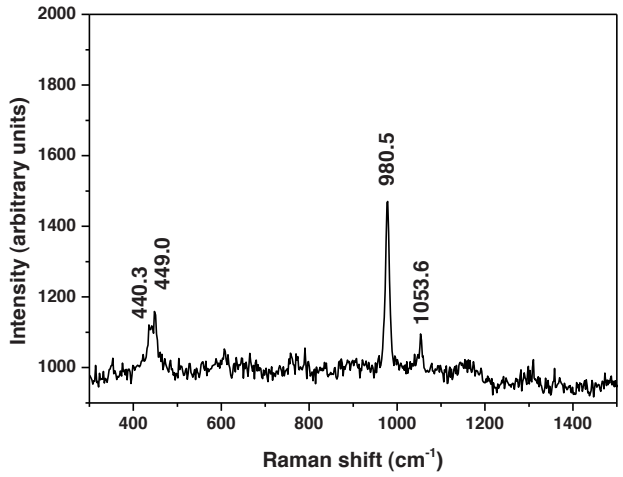

Figure 5.21. RLS anglesite Raman spectrum under 8 mbar CO_2 atmosphere at -20 °C.

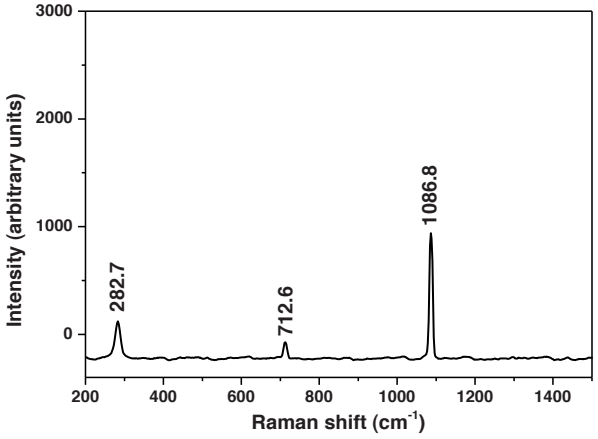

Figure 5.22. RLS calcite Raman spectrum at -20 °C under 8 mbar CO_2 atmosphere.

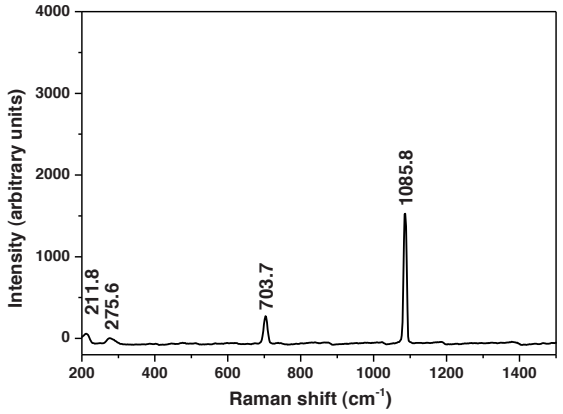

Figure 5.23. RLS aragonite Raman spectrum at -20 °C under 8 mbar CO_2 atmosphere.

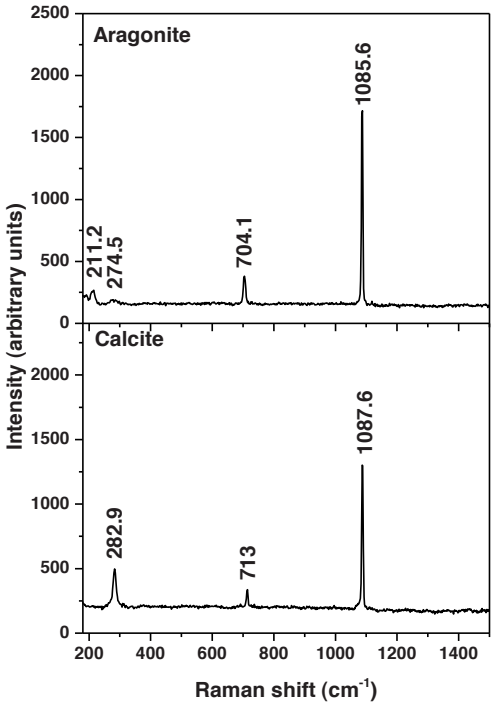

Figure 5.24. RLS Raman spectra of aragonite and calcite under vacuum at 10 °C in order to classify their mineral structure.

5.5 Raman data of selected hydrated sulphates and carbonates

5.5.1 Discussion on the Renishaw data of hydrated sulphates and carbonates

5.5.1.1 Renishaw Raman spectrum of gypsum ($CaSO_4 \cdot 2H_2O$)

Gypsum (calcium sulphate, $CaSO_4 \cdot 2H_2O$) has a layered structure. The atomic arrangement in the crystal structure comprises two sheets of sulphate ions that are closely bonded together by calcium ions (Ca^{2+}) to form strong double sheets in a repetitive mode. These sheets are held together by water molecules that share the two oxygen atoms with calcium in an octahedral structure. The water molecules hold the sheets together with hydrogen bonds.

The Raman spectrum of gypsum can be separated into two parts, which is shown in the Renishaw Raman spectrum in Fig. 5.4. The Raman spectrum of gypsum at frequency modes, < 400 cm^{-1}, caused by the external vibrations from both translator and rotator modes from sulphate, water groups and calcium. The vibrations of these bonds are between the Ca and the oxygen atoms of the sulphate ion and the bond between Ca and the oxygen of the water

molecules. Previous workers have proposed that the peak near 316 cm^{-1} is attributed to lattice vibration mode (Sarma et al., 1998).The weak Raman peaks caused by external vibrations were not detected in the Renishaw spectrum (Fig. 5.4).

Raman peaks in the region 400– 1200 cm^{-1} are attributed to internal vibrations of the sulphate groups. Previous studies indicate that these internal vibrations of the sulphate molecule are detected at frequencies above ~ 416 cm^{-1} with the last peak detected at ~ 1143 cm^{-1} (Sarma et al., 1998; Berenblut et al., 1971). Gypsum Raman spectrum obtained using the Renishaw (Fig. 5.4), yields the strongest Raman peak at 1007.1 cm^{-1}. This peak belongs to the ν_1 symmetric stretch vibration mode of the SO_4 tetrahedra. The peak at 1135.5 cm^{-1} corresponds to the ν_3 asymmetric stretch vibration mode. The ν_4 asymmetric bending vibration mode was detected as very weak peaks at 617.6 cm^{-1} and 669.6 cm^{-1}. The vibration modes at 413.9 cm^{-1} and 493.4 cm^{-1} show a pair of peaks related to ν_2 symmetric bending in the Renishaw Raman spectrum.

In gypsum Raman spectra, peaks in the spectral region > 3000 cm^{-1} describe the internal water group vibrations. The ν_1 and ν_3 vibration modes correspond to the symmetric and asymmetric stretching of the O– H bond and are present in Raman spectra in the 3300 to 3500 cm^{-1} region (Brotton and Kaiser, 2013). The Gypsum Renishaw spectrum showed peak at 3400.7 cm^{-1} for ν_1 as the signature of O– H vibration modes in our selected gypsum sample.

5.5.1.2 Renishaw Raman spectrum of barite ($BaSO_4$)

Renishaw spectrum of barite acquired under laboratory condition is presented in Fig. 5.5. The dominant intense peak, ν_1 symmetric stretching of SO_4 tetrahedra is detected at 989.8 cm^{-1}. The ν_3 asymmetric stretching vibration mode generates a peak at 1145 cm^{-1} and the peak at 462.2 cm^{-1} is attributed to the ν_2 bending vibration mode. The ν_4 asymmetric bending vibration mode generates a peak at 620.3 cm^{-1} in Renishaw barite spectrum.

5.5.1.3 Renishaw Raman spectrum of anglesite ($PbSO_4$)

The vibration modes of anglesite detected in the Renishaw spectrum are shown in Fig. 5.6. Renishaw spectrum demonstrates ν_1 symmetric stretching mode at 977.3 cm^{-1}. ν_2 bending vibration mode is characterise as a doublet peak at 438.3 and 449.5 cm^{-1}. A weak peak at 1053.5 cm^{-1}, is attributed to ν_3 vibration mode. Peaks at 605.2 and 640.9 cm^{-1} are attributed to the ν_4 asymmetric bending vibration mode.

5.5.1.4 Renishaw Raman spectrum of calcite ($CaCO_3$)

A calcite Raman spectrum determined by the Renishaw Raman microscope is shown in Figure 5.7. The calcite structure is well characterised with the dominant intense ν_1 symmetric stretching vibration mode of CO_3 group occurs at 1085.1 cm^{-1} and ν_4 at 711.5 cm^{-1}. Lattice vibration modes at 154.6 and 281.5 cm^{-1} are also distinguishable in this spectrum. The two

weak peaks at 1433.7 and 1746.9 correspond to the ν_3, asymmetric stretching mode and $2\nu_2$ vibration modes.

5.5.1.5 Renishaw Raman spectrum of aragonite ($CaCO_3$)

The Raman spectrum of aragonite obtained with the Renishaw Raman microscope is shown in Fig. 5.8. The characteristic Raman peak due to the ν_1 symmetric stretching mode of carbonate group at 1084.1 cm^{-1} is easily distinguished. The ν_4 mode of CO_3 has values at 703.5 cm^{-1}. The $2\nu_2$ vibration mode and ν_3 vibration mode, which appear in higher wavenumbers (> 1400 cm^{-1}), were not observed in the Renishaw spectrum. The peaks due to the external vibration modes of carbonate group are at 190.2, 210.4 and 273.1 cm^{-1}.

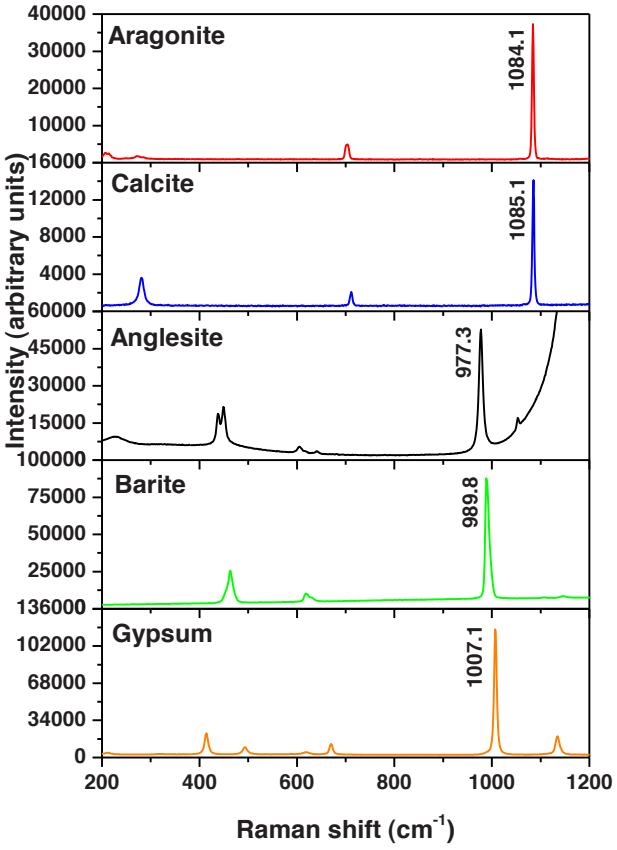

Figure 5.25.The Raman spectra of selected minerals taken with the Renishaw InVia Reflex confocal Raman microscope.

When the temperature of a sample is decreased, the bonds of the molecule usually become shorter. This means that, according to the Hook's law (see section 5.5.2.4) *k* (spring coefficient) increases. Consequently, Raman peaks might be affected by the temperature variations. Therefore, the peaks attributed to the symmetric stretching and asymmetric stretching vibration modes might have the most variation due to changes in the temperature. We might expect the peaks caused by stretching vibration modes as intensive and distinguishable peaks at 1084.1, 1085.1, 977.3, 989.8 and 1007.1 cm^{-1} in Raman spectra of aragonite, calcite, anglesite, barite and gypsum to be affected by the temperature variations (Fig. 5.25). Other peaks are so weak that we expect it will be hard to assess if there are small variations caused by lower temperature. We will study possible variations in Raman spectra due to the change in temperatures with the RLS instrument in the following section.

5.5.2 Discussion on the RLS data of hydrated sulphates and carbonates

5.5.2.1 RLS Raman spectrum of gypsum ($CaSO_4 \cdot 2H_2O$)

The RLS Raman spectrum of gypsum is presented in Fig. 5.9. RLS instrument detected two Raman peaks of gypsum (noise were appeared in shape of possible peaks in some part of this spectrum. However, they are not match to the peaks reported in the references). The strongest Raman peak at 1007.9 cm^{-1} is attributed to the ν_1 symmetric stretch vibration mode of the SO_4 tetrahedra. The peak at 493.3 cm^{-1} is related to ν_2 symmetric bending vibration mode. The detected peaks have a maximum error of ~ 0.8 cm^{-1} compared to the data reported in the Renishaw section. ν_4 and ν_3 were obscured in the strong background noise. Among of seven peaks detected via the Renishaw InVia Reflex confocal Raman microscope, RLS instrument detected the two strongest peaks (ν_1 and ν_2). RLS instrument was unable to fully focus on a grain of the selected gypsum sample. Our selected gypsum has grains in different optical orientations, which causes reflection of laser light in different directions. Therefore, the collection of the Raman emission was very week and we were unable to obtain a full Raman spectrum using RLS instrument. The RLS instrument cannot detect peaks in the spectral region > 3000 cm^{-1}. In order to detect the water molecular vibration, the effective operational range of the CCD detector must be re-scaled by either changing the angle of the grating or using a shorter wavelength laser source.

5.5.2.2 RLS Raman spectrum of barite ($BaSO_4$)

The RLS spectrum of barite is presented in Fig. 5.10. The main intense peak, ν_1 symmetric stretching vibration mode of SO_4 tetrahedra, occurs at 989.3 cm^{-1}. The peak at 461.6 cm^{-1} is attributed to the ν_2 bending vibration mode. The ν_3 asymmetric stretching vibration and ν_4 asymmetric bending vibration modes create peaks at 1144 cm^{-1} and 618 cm^{-1}. In the RLS Raman spectra, the four vibration modes of SO_4 correspond within error (~ 2 cm^{-1} to data reported above from the the Renishaw InVia Reflex confocal Raman microscope).

5.5.2.3 RLS Raman spectrum of anglesite ($PbSO_4$)

The vibration modes of anglesite detected with RLS instrument are shown in Fig. 5.11. RLS spectrum shows ν_1 symmetric stretching mode at 978.7 cm^{-1}. ν_2 bending vibration mode is determined as a doublet peak at 439.3 and 450.2 cm^{-1}. The RLS anglesite spectrum does not have well developed peaks with a flat base line. Multiple reflections from the sample surface made weak Raman peaks with low intensity (see section 6.2). ν_3 and ν_4 vibration modes were not detected in the RLS spectrum. In the Renishaw spectrum, these peaks were observed at a frequency of 1053.5 cm^{-1} (attributed to ν_3 vibration mode) and 605.2 and 640.9 cm^{-1} (attributed to the ν_4 vibration mode). The detected RLS Raman peaks match within an error of ~ 1.5 cm^{-1} with the data reported in Renishaw section.

5.5.2.4 A comparison of the internal vibrations of sulphate groups in anglesite and barite

In the mineral structure of sulphates, the size of the unit cell changes with composition. Replacements of cations with different mass, ionic radius and even different valency affect bond lengths and bond angle. These changes in the unit cell cause shifts in the frequencies of Raman peaks. Therefore the sulphate groups in barite and anglesite are expected to generate slightly different Raman peaks (Figs. 5.10 and 5.11). Table 5.2 shows that the RLS instrument is able to characterise these differences. In addition, the values of the four vibration modes of SO_4 match with data found in previous studies (Buzgar and Apopei, 2009; Beny, 1991; Dimova et al., 2006).

	Barite			Anglesite		
Vibration modes	RLS study	Buzgar et al., 2009	Dimova et, al., 2006	RLS study	Buzgar et al., 2009	Beny, 1991
ν_2 SO_4	461.6	461	453, 462	439.3, 450.2	450, 553	437, 449
ν_4 SO_4	618	619, 648	618, 647	ND*	611, 646	617, 640, 643
ν_1 SO_4	**989.3**	**989**	**988**	**978.7**	**978**	**977**
ν_3 SO_4	1144	1085,1143,1167	1140, 1167	ND*	1058, 1157	1051,1140, 1155

Table 5.2. Raman vibration peaks for barite and anglesite (cm^{-1}, * not detected).

As mentioned in chapter two, the molecular vibration modes are described as a function of the force constant of the vibration and the mass of the participating atoms. For a diatomic molecule, the vibrational frequency is described as Hook's law:

$$\nu = \frac{1}{2\pi c}\sqrt{\frac{k_0}{\mu}} \quad (5.1)$$

μ is reduced mass of participating atoms ($m_1m_2/(m_1+m_2)$), k_o is force constant in Newton per metre. ν is vibrational frequency in wave numbers. c is speed of light in centimetres per second. Therefore, according to Fadini and Schnepel (1989) the different sulphate vibration modes in barite and anglesite minerals are determined by differences in:

- Bond strength
- Atomic masses

In sulphates, ν_1 vibration mode depends on the S– O stretching force constant. The ν_1 vibration mode increases with an increase in the force constant. According to the study of Miyake et al. (1978), the stretching force constants for barite and anglesite are k = 6.27 and k = 5.98 md/A (md = millidyne, one dyne (1 dyn = 1 g·cm/s²) is defined as force F that accelerates an object with a mass of one gram one centimetre per second per second, Å angstrom, 1 Å = 0.1 nm). From equation 5.1, it is expected that the wavenumber decreases with an increase of the atomic mass of the cations. Table 5.3 presents ν_1 RLS Raman peak values for barite and anglesite, where the atomic masses of Ba and Pb are 137.32 and 207.2 u respectively. A comparison of the Raman spectra of barite and anglesite illustrates that the value of ν_1 decreases with an increase of the atomic mass of the major metal ion in the lattice. Data from RLS study therefore agrees with the predictive model of Fadini and Schnepel (1989) discussed above. Given the diverse nature of sulphate mineralogy reported from Mars we expect that this model will be useful in classifying the structure of sulphates with different atomic masses on Mars. However, it should be kept in mind that, the variation in peak positions could potentially be caused by temperature changes. Hence, this matter is investigated in the following sections.

5.5.2.5 Raman spectra of gypsum, barite and anglesite at low temperature under 8 mbar CO_2 pressure and vacuum conditions.

The mineral structure of gypsum, barite and anglesite were studied with the RLS instrument at -20 °C under two different conditions: i) 4 x 10^{-5} mbar vacuum condition, ii) 8 mbar CO_2 pressure.

i) 4 x 10^{-5} mbar vacuum condition: RLS Raman spectra obtained at -20 °C were compared to RLS Raman spectra obtained at 10 °C (Figs. 5.14, 5.15 and 5.16).

The wavenumbers of the resolved peaks for vibration modes of each mineral are summarised in Table 5.3. Their Raman spectra obtained at -20 °C under vacuum condition, are all within ~ 0.3 wavenumber of those acquired at 10 °C under vacuum condition. Therefore we conclude that we are unable to detect any significant change in Raman spectra related to temperature change. However, we should keep in mind that depending on mineral symmetry, shifts in Raman spectra of specific minerals have been reported at much lower temperatures (-253 °C ; Weber et al., 2012). Hence for the unambiguous detection of carbonates and sulphate minerals on planetary bodies without an atmosphere and under more extreme temperature conditions extensive further experimentation is required.

	Barite		Gypsum		Anglesite	
Vibration modes	-20 °C	10 °C	-20 °C	10 °C	-20 °C	10 °C
ν_2 SO_4	461.6	461.6	493.6	493.3	439.8, 449.9	439.3, 450.2
ν_4 SO_4	618.3, 631.4	618	ND*	ND*	ND*	ND*
ν_1 SO_4	989.7	989.3	1008.1	1007.9	979.1	978.7
ν_3 SO_4	1144.9	1144	ND*	ND*	1054	ND*

Table 5.3. RLS Raman peaks for barite, gypsum and anglesite at -20 and 10 °C under vacuum, * not detected.

As explained in section 3.6.3, the inefficient cooling of the CCD in the RLS instrument means that the minimum temperature reached by the CCD depends on the atmospheric conditions in the MASC. CCD reached its lowest temperature (~ -41.2 °C) when we obtained RLS Raman spectra under vacuum condition at -20 °C. Therefore, the CCD thermal background noise was lower and allowed resolution of some weak peaks. For example in the barite RLS Raman spectrum acquired at -20 °C, one of the weak peaks, which is attributed to ν_4 vibration mode of the sulphate group, was detected at 631.4 cm^{-1}. However, this peak was not observed in the barite RLS Raman spectra obtained at 10 °C when the CCD temperature was -31.4 °C. Similarly, different peaks are resolved in the RLS Raman spectra of anglesite at -20 and 10 °C under vacuum condition. At -20 °C, a weak peak at 1054 cm^{-1}, which is attributed to ν_3 vibration mode of the sulphate group, is resolved. This peak is not detected at 10 °C. Noise levels varied from 3 to 5 when the CCD was operating at temperatures of ~ -30 and -40 °C respectively.

ii) 8 mbar CO_2 pressure (Martian conditions): Raman spectra obtain at -20 °C under 8 mbar CO_2 pressure were compared to RLS Raman spectra obtain at -20 °C under 4 x 10^{-5} mbar vacuum conditions (Figs. 5.19, 5. 20 and 5. 21).

Data presented in table 5.4, establishes that the Raman peaks obtained under Martian conditions are all within ~ 1 wavenumber of those obtained under vacuum condition and consequently we can conclude that we are unable to detect any significant change in Raman spectra related to temperature and pressure changes applicable to the operational conditions.

	Barite		Gypsum		Anglesite	
Vibration modes	4 x 10^{-5} mbar	8 mbar CO_2	4 x 10^{-5} mbar	8 mbar CO_2	4 x 10^{-5} mbar	8 mbar CO_2
ν_2 SO_4	461.6	461.5	493.6	492.8	439.8, 449.9	440.3, 449
ν_4 SO_4	618.3, 631.4	618.1	ND*	ND*	ND*	ND*
ν_1 SO_4	989.7	989.0	1008.1	1008.8	979.1	980.5
ν_3 SO_4	1144.9	1144.2	ND*	ND*	1054	1053.6

Table 5.4. RLS Raman peaks for barite, gypsum and anglesite at -20 °C under vacuum and at 8mbar CO_2, * not detected.

5.5.2.6 RLS Raman spectrum of calcite ($CaCO_3$)

The RLS calcite spectrum is presented in Fig. 5.12. The Raman spectra of calcite is characterised by the most intensive ν_1 symmetric stretching of CO_3 group at 1087.6 cm^{-1}, ν_4 symmetric bending mode is shown at 713 cm^{-1} and one lattice vibration mode at 282.9 cm^{-1}.These peaks are within ~ 2 cm^{-1} of the data reported in the Renishaw section. The possible $2\nu_2$ and ν_3 peaks, which were detected with the Renishaw Raman microscope, were not detected with the RLS instrument. These weak peaks appear to have been obscured within the background noise.

5.5.2.7 RLS Raman spectrum of aragonite ($CaCO_3$)

Figure 5.13 shows the RLS aragonite spectrum. The spectrum has well-formed peaks with a flat base line. The observed peaks in this spectrum are as follow: ν_1 as the very strong Raman peak at 1085.6 cm^{-1}, ν_4 vibration mode with the value of 704.1 cm^{-1} and two weak lattice vibration modes at 211.2 and 274.5 cm^{-1}. The resolved peaks have the same value within ~ 2 cm^{-1} of the data presented in Renishaw section. In RLS Raman study, the $2\nu_2$ and ν_3 vibration modes were not observed. The detection of the $2\nu_2$ vibration mode and ν_3 vibration mode (> 1400 cm^{-1}) of aragonite was also impossible with the Renishaw InVia Raman microscope.

5.5.2.8 A comparison between calcite and aragonite RLS Raman spectra

A comprehensive study of the calcite and aragonite spectra is reported by Couture 1947; Krishnamurti 1956, 1957; Porto et al., 1966; Griffith 1969; Rutt and Nicola 1974; White 1974; Frech et al., 1980; Bischoff et al., 1985. The principal Raman peak of both calcite and aragonite is produced by the internal vibrations of the carbonate ion, which is an essential component of both calcite and aragonite. It is therefore expected that the ν_1 vibration mode of CO_3 group may be indistinguishable between the two minerals. We present the RLS Raman spectra of aragonite and calcite in Figure 5.24. ν_1 vibration modes occurred at 1087.6 cm^{-1} and 1085.6 cm^{-1} in calcite and aragonite RLS Raman spectra respectively. As the two minerals are not pure end-member compositions but contain additional elements such as Mg, Mn and Sr, it is impossible to establish if the small (~ 2 cm^{-1}) differences between ν_1 vibration modes of calcite and aragonite are caused by compositional variations of minor elements or the minerals themselves. Further work on pure endmember compositions are required to resolve this question.

The shorter wavenumber peaks, however, are significantly different in the RLS Raman spectra of calcite and aragonite (Table 5.6). The lower wavenumber peaks are attributed to the vibrations of the ionic arrangement within the crystals. These peaks present the characteristic differences in Raman spectra of the two minerals (White, 1974). In our work, we can clearly observe the predicted differences between lattice vibration modes at 282.9 and 274.5 cm^{-1} in calcite and aragonite (Figure 5.24). The difference is ~ 8.4 cm^{-1}. ν_4 modes at 713 cm^{-1} in the calcite RLS spectrum and 704.1 cm^{-1} in aragonite RLS spectrum have a difference of ~ 8.9 cm^{-1}. Therefore, we can conclude that with the RLS instrument, we have identified the similarities and differences in the RLS Raman spectra of aragonite and calcite.

5.5.2.9 RLS Raman spectra of calcite and aragonite at low temperature under 8 mbar CO_2 pressure and vacuum condition.

In this section, we study the mineral structure of calcite and aragonite with the RLS instrument at -20 and 10 °C under vacuum condition. Our goal is to identify any possible structural changes in the mineral lattice of calcite and aragonite at low temperature by identifying Raman shifts. In subsequent experiments, we have analysed the mineral structure of calcite and aragonite under 8 mbar CO_2 pressure and vacuum condition at -20 °C. Our goal is to monitor the possible effect of Martian conditions on RLS Raman spectra of calcite and aragonite.

Peaks in the Raman spectra of calcite and aragonite under vacuum condition at -20 °C (are respectively) within ~ 0.5 and 1 cm^{-1} of spectra obtained under vacuum condition at 10 °C (Figs 5.17 and 5.18). We conclude that there are no detectable shifts due to the low temperature. As we discussed in section 5.5.2.5, for the clear detection of carbonates and sulphate minerals on planetary bodies without an atmosphere further low temperature experimentation is needed.

Table 5.5 demonstrates that peaks resolved in the Raman spectra obtained under Martian conditions are within ~ 1 cm^{-1} of those obtained under vacuum condition. As a result, we can again conclude that there are no resolvable differences in Raman spectra related to pressure changes.

	Calcite		Aragonite	
Vibration modes	4 x 10^{-5} mbar	8 mbar CO_2	4 x 10^{-5} mbar	8 mbar CO_2
ν_1	1087.4	1086.8	1086.9	1085.8
ν_4	713.2	712.6	703.7	703.7
Lattice vibration mode	282.7	282.7	211.2, 273.7	211.8, 275.6

Table 5.5. RLS Raman peaks for calcite and aragonite (cm^{-1}) under vacuum (10^{-5} mbar) and at 8 mbar CO_2 at -20 °C.

5.6 Conclusion

This study describes the successful application of the RLS instrument to detect sulphate and carbonate minerals under Marian conditions. We investigated if the temperature affects some of the vibration modes in selected mineral structure.

The Raman peaks obtained with the RLS instrument under vacuum conditions at -20 °C inside MASC chamber are indistinguishable to those obtain with Renishaw InVia Reflex confocal Raman microscope and data reported in the literature. These data indicated the accurate performance and calibration of the RLS instrument at lower temperatures. Moreover, Raman spectra obtained under Martian conditions (8 mbar CO_2 pressure and -20 °C) are indistinguishable to those obtained under vacuum conditions at temperature of -20

°C. These data establish that there is no significant shift in Raman peaks of carbonates and sulphates under Martian conditions. Significantly, this means that Raman spectra of these minerals obtained in the ExoMars rover will be indistinguishable from terrestrial spectra and for carbonates a standard terrestrial derived database can be used for the identification of carbonate minerals.

RLS Raman spectra for barite, anglesite and gypsum have clear differences that can be related to the different mineral structures. In all spectra, there were variations in peak positions and peak splitting due to the influences of the different metal cations. In the case of barite and anglesite, the wavenumber of the vibrational modes of SO_4 tetrahedra, decreases with an increase of the atomic mass of the metal cations. In addition, Raman peaks shift to higher wavenumbers with an increase of the stretching force constant of S– O bonds.

The water vibration mode is detected in the Renishaw Raman gypsum spectrum. However, we could not identify any water vibration mode in RLS Raman gypsum spectrum. Therefore, we can conclude that the design of the RLS instrument is not optimal. To detect the vital component of hydrated minerals we suggest a redesign of the RLS instrument. To detect this molecular vibration, the range of the CCD detector must be re-scoped by either changing the angle of the grating or applying a shorter wavelength laser source (see chapter six for more discussion).

The purpose of the study of calcite and aragonite with the RLS instrument was to highlight the possibility for the analysis of polymorph minerals with the RLS instrument. We have shown that the RLS instrument is a useful device for the determination of polymorphs under Martian conditions.

5.7 References

Bandfield, J. L. et al., (2003), Spectroscopic Identification of Carbonate Minerals in the Martian Dust.Science, Vol. 301, p.1084.

Beny, C. (1991), Société Française de Minéralogie et de Cristallographie - Base de données de spectres Raman. Anglesite. (http://wwwobs.univ-bpclermont.fr /sfmc/ramandb2/fpdf/ANGLE11.pdf).

Berenblut B. J., P. Dawson and B. R. Wilkinson, (1971), The Raman spectrum of gypsum. Spectrochimica, Acta A., 27(9), p. 1849-1863.

Bischoff W. D., S. K. Sharma, F. T. Mackenzie, (1985), Carbonate ion disorder in synthetic and biogenic magnesian calcites: a Raman spectral study. Am Mineral 70, p. 581-589.

Bridges, J. C. et al., (2001), Alteration assemblages in Martian meteorites: implications for near-surface processes. Space Sci. Rev. 96, p. 365–392.

Brotton S. J. and R. I. Kaiser, (2013), In Situ Raman Spectroscopic Study of Gypsum (CaSO4&middot2H2O) and Epsomite (MgSO4&middot7H2O) Dehydration Utilizing an Ultrasonic Levitator .JPCL, 4, p. 669-673.

Buzgar, N., A. I. Apopei, (2009), The Raman study on certain carbonates. Iasi, Tome 55, issue 2, p. 97-112.

Catling, D. C. (1999), A chemical model for evaporites on early Mars: Possible sedimentary tracers of the early climate and implications for exploration, Journal of Geophys. Res., 104, 16,453-16,470.

Christensen, P. R. et al., (2004), Mineralogy at Meridiani Planum from the Mini-TES experiment on the Opportunity rover, Science, Vol. 306, p. 1733–1739.

Couture, L. (1947) Etude des spectres de vibrations de monocristaux ioniques. Annales de Physique, 2(12), 5-94.

Dimova, M., G. Panczer, M. Gaft, (2006), Spectroscopic study of barite from the Kremikovtsi deposit (Bulgaria) with implication for its origin. Annales Géologiques de la Péninsule Balkanique, Vol. 67, p. 101-108.

Fairen, A. G. et al., (2004), Inhibition of carbonate synthesis in acidic oceans on early Mars, Nature 431, p. 423.

Frech R, E. C. Wang, J. B. Bates, (1980), The IR and Raman spectra of CaCO3 (aragonite). Spectrochim Acta 36A, p. 915-919.

Gooding, J. L. (1978), Chemical weathering on Mars thermodynamic stabilities of primary minerals (and their alteration products) from mafic igneous rocks. Vol. 33, Issue 3, p. 483–513.

Griffith W. P. (1969), Raman spectroscopy of minerals. Nature 224, p. 264-266.

Griffith W. P. (1970), Raman studies on rock-forming minerals. II. Minerals containing MO3, MO4 and MO6 groups. Journal of Chem. Soc. A(2), 286-91.

Gunasekaran. S, G. Anbalagan, S. Pandi, (2006), Raman and infrared spectra of carbonates of calcite structure. Journal of Raman Spectroscopy, Vol. 37, p. 892-899.

Hannington, M. D. and D. Steven, (1988) Scott Mineralogy and geochemistry of a hydrothermal silica-sulfide-sulfate spire in the caldera of Axial Seamount, Juan De Fuca RidgeCan Mineral, Vol. 26, p. 603-625.

Haymon, R. M., (1983), Growth history of hydrothermal black smoker chimneys, Nature 301, 695 - 698; DOI:10.1038/301695a0.

Krishnamurti, D. (1956), Raman spectrum of magnesite. Proc Indian Ac Sci A43:210-212.

Krishnamurti, D. (1957), The Raman spectrum of calcite and its interpretation. Proc Indian Ac Sci A46, p. 183 202.

Langevin, Y., F. Poulet, J. P. Bibring, B. Gondet, (2005), Sulphates in the North Polar Region of Mars Detected by OMEGA/Mars Express. Science, Vol. 307, no. 5715, p. 1584-1586.

Mitra S. S. and P. J. Gielisse, (1964), Progress in Infrared Spectroscopy (Plenum Press, Inc., New York,), Vol. 2, pp. 47-125.

Nakamoto, K. (2009), Infrared and Raman Spectra of Inorganic and Coordination Compounds Part A: Theory and Applications in Inorganic Chemistry (Sixth edition). John Wiley and Sons, New Jersey.

Porto S. P. S, J. A. Giordmaine, T. C. Damen, (1966), Depolarization of Raman scattering in calcite. Phys Rev 147, p. 608-611.

Rachel M. Haymon and M. Kastner, (1981), Hot spring deposits on the East Pacific Rise at 21°N: preliminary description of mineralogy and genesis, Earth and Planetary Science Letters, Vol. 53, Issue 3, p. 363–381.

Ramakrishnan, V., V. U. Nayar, G. Aruldhas, (1985), Vibrational spectra of LiRbSO4 Infrared Phys. 25 (4), p. 607–610.

Rutt, H. N., J. H. Nicola, (1974), Raman spectra of carbonates of calcite structure. Journal of Phys C 7, p. 4522-4528.

Sarma, L. P., P. S. R. Prasad, N. Ravikumar, (1998). Raman Spectroscopic Study of Phase Transitions in Natural Gypsum. Journal of Raman Spectroscopy, Vol. 29, p. 851-856.

Skinner, B. J., S. C. Porter, (1989), The dynamic earth: an introduction to physical geology, pp. 540.

Squyres, S.W. et al., (2004), The Opportunity Rover's Athena Science Investigation at Meridiani Planum, Mars. Science 306, 1698. Vol. 306, no. 5702, pp. 1698-1703.

Tivey M. K., R. E. McDuff, (1990), Mineral precipitation in the walls of black smoker chimneys: a quantitative model of transport and chemical reaction. Journal of Geophys. Res., Vol. 95, p. 12617-12637.

Weber, I. et al., (2012), Raman spectroscopy of Mars relevant and minerals for planetary exploration, 43rd Lunar and Planetary Science Conference, 1793.

White, W. B. (1974), The carbonate minerals. In V. C. Farmer, Ed., The Infrared Spectra of Minerals, Mineralogical Society Monograph 4, p. 227-284.